Research Square

Preprints are preliminary reports that have not undergone peer review.
They should not be considered conclusive, used to inform clinical practice,
or referenced by the media as validated information.

Proteomic identification of secreted protein candidates mediating anti-colorectal cancer activity in a human-derived non-enterotoxigenic Bacteroides fragilis

Yiting Peng
Zunyi Medical University
Lian Huang
Zunyi Medical University
Mingzhu Chen
Zunyi Medical University
Hao Yang
Chongqing Mental Health Center, Liangjiang New Area
Yu Gan
Zunyi Medical University
Ningyan Wang
Zunyi Medical University
Maijian Wang
Institute of Gastroenterology, Affiliate Hospital of Zunyi Medical University
Zhongmin Yang
Zunyi Medical University
Jida Li
lijida198485@163.com
Zunyi Medical University

Research Article

Keywords: Bacteroides fragilis, colorectal cancer, activity-guided fractionation, proteomics, membrane-associated proteins, microbiota-derived therapeutics

Posted Date: July 3rd, 2026

DOI: https://doi.org/10.21203/rs.3.rs-10101527/v1

License: This work is licensed under a Creative Commons Attribution 4.0 International License. Read Full License

Additional Declarations: No competing interests reported.

Version of Record: A version of this preprint was published at BMC Cancer on October 5th, 2026. See the published version at https://doi.org/10.1186/s12885-026-17063-2.

Abstract

The contribution of gut microbiota-derived factors to colorectal cancer (CRC) progression has attracted increasing attention; however, the specific bioactive components and their underlying mechanisms remain poorly defined. In this study, an activity-guided fractionation approach combined with proteomic analysis was employed to identify anti-CRC components derived from a human-origin, non-enterotoxigenic *Bacteroides fragilis* strain. Bacterial conditioned supernatant was sequentially fractionated by ultrafiltration, solvent extraction, and chromatography, and the antiproliferative activity of each fraction was evaluated in HT-29 cells. Active fractions were subsequently subjected to LC–MS/MS analysis and bioinformatic characterization. A total of 41 proteins were significantly enriched in the bioactive fractions. Functional annotation revealed that these proteins were primarily involved in iron acquisition, ATP-binding cassette (ABC) transport systems, and protein secretion pathways. Notably, a substantial proportion of these proteins were predicted to be localized to the outer membrane or to contain signal peptides, indicating potential roles in host–microbe interactions. The observed anti-proliferative effects are likely attributable to the synergistic action of multiple proteins rather than a single effector molecule. Collectively, these findings provide novel insights into the molecular mechanisms underlying microbiota-derived anti-cancer activity and establish a basis for the development of microbiota-based therapeutic strategies for CRC.

1. Introduction

Colorectal cancer (CRC) continues to represent one of the most prevalent and deadly malignancies worldwide, posing a substantial and escalating global health burden[1, 2]. According to recent epidemiological data, CRC ranks among the top three cancers in both incidence and mortality, accounting for approximately 1.9 million new cases and 900,000 deaths annually[1]. Although advances in screening and early detection in developed regions have contributed to a stabilization or decline in incidence among older populations, a concerning rise in early-onset CRC among individuals under 50 years of age has emerged as a significant clinical challenge[3, 4]. Furthermore, population aging and prolonged exposure to environmental and lifestyle-related risk factors are expected to drive a continued increase in CRC incidence globally in the coming decades[5].Current treatment modalities, including surgical resection, chemotherapy, targeted therapy, and immunotherapy, have improved clinical outcomes to a certain extent. Nevertheless, their overall effectiveness remains constrained by factors such as drug resistance and intratumoral heterogeneity[6, 7]. Notably, most patients with microsatellite-stable CRC demonstrate limited responsiveness to immune checkpoint blockade[8, 9], underscoring the pressing need to develop alternative or adjunctive therapeutic strategies with enhanced efficacy, safety, and broader clinical applicability.

The human gut microbiota, often described as a “second genome,” plays an essential role in host metabolism, immune regulation, and the maintenance of intestinal homeostasis, and has increasingly been recognized as a key modulator of colorectal cancer (CRC) initiation and progression[10]. Accumulating evidence suggests that the gut microbiota contributes to colorectal carcinogenesis not only through alterations in community composition but also via its functional outputs, including metabolites and secreted bioactive molecules.While microbially derived metabolites, such as secondary bile acids, have been extensively implicated in tumor promotion through inflammatory and metabolic mechanisms[11, 12], emerging studies indicate that bacterial secreted proteins can function as direct effectors in host–microbe interactions, These proteins are capable of influencing host signaling pathways, modulating immune responses, and altering cellular behaviors relevant to tumorigenesis[13]. Notably, certain probiotic-derived proteins, exemplified by the P8 protein from *Lactobacillus rhamnosus*, have been demonstrated to suppress CRC cell proliferation and migration, thereby supporting the concept that microbial secretomes represent a promising source of anti-cancer agents[14].Despite these advances, research has predominantly focused on microbial metabolites, and the systematic identification and functional characterization of proteinaceous effectors derived from gut commensal bacteria remain relatively limited.

Bacteroides fragilis, a prevalent anaerobic commensal of the human colon, exhibits a context-dependent dual role in host physiology and disease[15]. Enterotoxigenic *B. fragilis* (ETBF) strains produce *B. fragilis* toxin (BFT), a metalloprotease that disrupts epithelial barrier integrity and promotes inflammation-driven tumorigenesis[16], and have been consistently associated with an increased risk of colorectal cancer (CRC) in both experimental models and epidemiological studies[17, 18]. In contrast, non-toxigenic *B. fragilis* (NTBF) strains lack BFT and are generally regarded as beneficial commensals, contributing to immune modulation and the maintenance of intestinal homeostasis, For example, polysaccharide A (PSA) derived from NTBF has been shown to induce regulatory T cell responses and attenuate inflammation[16, 19].Recent studies further suggest that specific NTBF strains may exert anti-tumor effects, potentially through modulation of host immunity[20]. However, the molecular mechanisms underlying these protective effects remain insufficiently characterized. In particular, it remains unclear whether NTBF secretes proteinaceous factors with direct anti-CRC activity, and the identity and functional properties of such molecules have yet to be systematically elucidated.

In this study, a human-derived non-toxigenic *Bacteroides fragilis* (NTBF) strain, ZY0804, previously isolated from para-carcinoma tissue, was investigated because its cell-free supernatant exhibited marked inhibitory effects on HT-29 colorectal cancer cells[21]. To systematically identify the bioactive components responsible for this activity, a bioactivity-guided fractionation strategy was employed that integrated ultrafiltration, size-exclusion chromatography, ion-exchange chromatography, solvent partitioning, and reverse-phase high-performance liquid chromatography. The resulting bioactive fractions were subsequently analyzed by liquid chromatography–tandem mass spectrometry (LC–MS/MS), followed by comparative proteomic profiling using adjacent inactive fractions as controls. Candidate proteins were prioritized on the basis of differential enrichment, peptide support, and predicted subcellular localization, and were further characterized through functional annotation and protein–protein interaction network analysis.This study was designed to determine the physicochemical basis of NTBF-derived anti-CRC activity, to enrich and isolate bioactive fractions through activity-guided purification, to identify candidate protein effectors by comparative proteomics, and to provide mechanistic insight into the anti-cancer effects mediated by NTBF. Collectively, these findings establish a systematic framework for the discovery of microbiota-derived anti-tumor proteins and provide a prioritized set of candidates for future functional validation.

2. Materials and methods

2.1. Bacterial strain and culture conditions

Bacteroides fragilis strain ZY0804 (GenBank accession no. CP139161), originally isolated from adjacent non-tumorous tissue of patients with colorectal cancer, was maintained in our laboratory.For recovery, the strain was revived from − 80°C glycerol stocks by inoculating 200 µL of bacterial suspension into 10 mL of brain heart infusion (BHI) broth supplemented with hemin (5 µg/mL) and vitamin K1 (1 µg/mL). The cultures were incubated anaerobically at 37°C for 48 h using an anaerobic cultivation system.For large-scale cultivation, 1 mL of the activated culture was transferred into 500 mL of BHI broth and incubated under anaerobic conditions at 37°C for 24–48 h until the logarithmic growth phase was reached. Bacterial density was determined by serial dilution followed by colony counting on BHI agar plates under anaerobic conditions.

2.2. Preparation of bacterial conditioned supernatant (BfCFS)

Bacterial cultures were centrifuged at 4°C (4,500 rpm for 25 min) to remove bacterial cells. The resulting supernatant was then passed through 0.45 µm sterile filters to obtain cell-free supernatant, designated as BfCFS. The filtered BfCFS was aliquoted and stored at − 80°C until further use.

2.3. Ultrafiltration-based fractionation

BfCFS (10 mL) was subjected to ultrafiltration using centrifugal filter units with a 10 kDa molecular weight cut-off. The samples were centrifuged at 4°C with stepwise increases in speed (3,000 rpm for 15 min, 3,500 rpm for 10 min, and 4,000 rpm for 5 min) until an approximately 10-fold concentration was achieved. The retentate (> 10 kDa) and filtrate (< 10 kDa) were collected separately. The > 10 kDa fraction was desalted by three repeated dilution–concentration cycles with phosphate-buffered saline (PBS). Both fractions were subsequently assessed for anti-proliferative activity.

2.4 Organic solvent extraction

BfCFS was mixed with ethyl acetate at a 1:2 (v/v) ratio and subjected to liquid–liquid extraction. Following vigorous mixing and phase separation, the aqueous and organic phases were collected separately. The aqueous phase was then concentrated under reduced pressure at 40°C and reconstituted in sterile water for subsequent fractionation.

2.5 Size-exclusion chromatography (SEC)

The > 10 kDa fraction was further separated by size-exclusion chromatography using a Sephacryl S-200 HR column (15 mm × 60 cm). The column was equilibrated with buffer containing 20 mM Tris-HCl, 150 mM NaCl, and 5% glycerol (pH 7.4), and chromatography was performed at a flow rate of 0.5 mL/min. Elution was monitored at 280 nm, and fractions were collected automatically. Based on the elution profile, the collected fractions were pooled and designated Fr.A1–Fr.A3 for subsequent bioactivity screening.

2.6 Ion-exchange chromatography

The bioactive fractions obtained by size-exclusion chromatography (SEC) were further subjected to ion-exchange chromatography. For anion-exchange separation, samples were loaded onto a HiTrap Q HP column pre-equilibrated with 20 mM Tris–HCl buffer (pH 7.4), and elution was carried out using stepwise and linear gradients of NaCl (0–1 M). For cation-exchange separation, samples were applied to a

HiTrap SP HP column equilibrated with 20 mM sodium phosphate buffer (pH 5.0). Fractions were collected at 1 mL intervals and subsequently evaluated for bioactivity.

2.7 Reverse-phase HPLC (RP-HPLC)

The < 10 kDa fraction was desalted by C18 solid-phase extraction and subsequently further separated by reverse-phase high-performance liquid chromatography (RP-HPLC) using an Agilent 1260 Infinity II system. Chromatographic separation was carried out on a C18 column with a linear acetonitrile gradient (5–80%) containing 0.1% trifluoroacetic acid (TFA). Elution was monitored at 220 and 280 nm. The resulting fractions were collected, lyophilized, reconstituted, and then subjected to biological activity evaluation.

2.8. Cell culture and treatment

Human colorectal cancer HT-29 cells were obtained from the Cell Bank of the Chinese Academy of Sciences. The cells were maintained in RPMI-1640 medium supplemented with 10% fetal bovine serum and 1% penicillin–streptomycin in a humidified incubator at 37°C with 5% CO_2. Cells were routinely passaged at 80–90% confluence using 0.25% trypsin.

2.9. Cell viability and proliferation assays

Cell viability and proliferative capacity were assessed using Cell Counting Kit-8 (CCK-8), colony formation, and EdU incorporation assays. For the CCK-8 assay, HT-29 cells were seeded into 96-well plates at a density of 5×10^3 cells per well and allowed to adhere for 12 h. The cells were then treated with the indicated fractions for 48 h. Subsequently, 100 μL of CCK-8 working solution was added to each well, followed by incubation for 2 h, and absorbance was measured at 450 nm using a microplate reader.For the colony formation assay, HT-29 cells were seeded into 6-well plates at a density of 1×10^3 cells per well and treated for 48 h. The medium was then replaced with fresh complete medium, and the cells were cultured for an additional 7–10 days to allow colony formation. The resulting colonies were fixed with 4% paraformaldehyde, stained with crystal violet, and counted.Cell proliferation was further evaluated using an EdU incorporation assay kit according to the manufacturer's instructions. Fluorescence images were captured using a fluorescence microscope, and the proportion of EdU-positive cells was quantified.

2.10. LC–MS/MS-based proteomic analysis

Proteomic profiling of the active and inactive fractions was conducted using an LC–MS/MS-based workflow. Protein samples were first reduced with 10 mM dithiothreitol (DTT) and alkylated with 25 mM iodoacetamide, followed by overnight tryptic digestion at 37°C using an enzyme-to-protein ratio of 1:50. The resulting peptides were purified by C18 solid-phase extraction before mass spectrometric analysis.Purified peptides were analyzed using a nano-liquid chromatography system coupled to a Q Exactive mass spectrometer. Peptide separation was performed on a C18 analytical column using a linear acetonitrile gradient containing 0.1% formic acid at a flow rate of 300 nL/min. Mass spectrometric data were acquired in data-dependent acquisition (DDA) mode.Raw MS data were processed using PEAKS Studio version 11.0 and searched against the *Bacteroides fragilis* protein database retrieved from UniProt. Trypsin was specified as the digestion enzyme, with up to two missed cleavages permitted. The precursor ion mass tolerance was set to 10 ppm, and the fragment ion mass tolerance was set to 0.02 Da. Protein identifications were accepted at a false discovery rate (FDR) of ≤ 1%.

2.11. Bioinformatics analysis

Proteins significantly enriched in the active fractions were identified through quantitative proteomic analysis. Fold change (FC) values were calculated by comparing protein abundances between active fractions and their corresponding inactive controls, and proteins with an FC ≥ 2.0 were defined as enriched.Functional annotation was performed using Gene Ontology (GO) classification, categorizing proteins into biological process, molecular function, and cellular component. Enrichment patterns were summarized based on the distribution and proportion of proteins within each category.Protein family classification and conserved domain analysis were conducted using publicly available databases, including Pfam, SUPERFAMILY, and UniProt. Proteins were grouped into functional families according to their domain architecture and annotation profiles.Subcellular localization was predicted using PSORTb, and the presence of signal peptides was assessed using SignalP 6.0 to evaluate the potential for protein secretion.A functional association network was constructed and visualized using Cytoscape. Protein–protein interactions were inferred based on shared functional annotations, pathway co-membership, and literature-supported associations. Network topology parameters, including node degree, were calculated to evaluate protein connectivity and to identify key hub proteins.Candidate proteins were prioritized through an integrative analysis incorporating multiple criteria, including degree of enrichment, functional annotation, predicted subcellular localization, and network connectivity.

2.12. Statistical analysis

All experiments were conducted with a minimum of three independent replicates. Data are presented as the mean ± standard deviation (SD). Statistical analyses were performed using SPSS software (version 29.0). Differences among groups were evaluated using one-way analysis of variance (ANOVA) followed by the least significant difference (LSD) post hoc test, or the Kruskal–Wallis test when appropriate. A p-value < 0.05 was considered to indicate statistical significance.

3. Results

3.1 BfCFS inhibits proliferation of colorectal cancer cells

To assess the anti-proliferative effects of cell-free supernatant derived from *Bacteroides fragilis* ZY0804 (BfCFS), HT-29 cells were treated with BfCFS and evaluated using multiple complementary assays. CCK-8 analysis showed that BfCFS treatment significantly reduced cell viability to 54.68% of the untreated control, corresponding to an inhibition rate of 45.32% ($P < 0.001$), whereas no significant change was observed in the BHI medium control group ($P > 0.05$) (Fig. 1A).Consistent with these findings, colony formation assays demonstrated a significant decrease in clonogenic capacity, with colony numbers reduced to 59.61% of the control ($P < 0.01$) (Fig. 1B), indicating impaired long-term proliferative potential. At the single-cell level, EdU incorporation assays further confirmed the inhibitory effect on DNA synthesis, with the proportion of EdU-positive cells decreased by 32.75% compared with the control ($P < 0.001$). No significant difference was detected between the BHI and control groups (Fig. 1C).Taken together, these results indicate that BfCFS exerts a pronounced inhibitory effect on the proliferation of colorectal cancer cells.

3.2 Bioactivity is predominantly associated with > 10 kDa fractions

To characterize the physicochemical properties of the bioactive components, BfCFS was fractionated using a 10 kDa molecular weight cutoff. CCK-8 analysis revealed that the > 10 kDa fraction retained significant anti-proliferative activity, comparable to that of the unfractionated BfCFS ($P < 0.001$), whereas the < 10 kDa fraction did not produce a significant effect ($P > 0.05$) (Fig. 2A).These findings were further corroborated by colony formation and EdU incorporation assays. Only the > 10 kDa fraction significantly reduced clonogenic survival and DNA synthesis ($P < 0.001$), while the < 10 kDa fraction showed no detectable inhibitory activity (Figs. 2B,C).Collectively, these results indicate that the anti-colorectal cancer activity of BfCFS is primarily associated with macromolecular components with molecular weights greater than 10 kDa.

3.3 Sequential chromatographic fractionation enriches active components

3.3.1 Size-exclusion chromatography identifies active fraction

The > 10 kDa fraction was further separated by Sephacryl S-200 size-exclusion chromatography, yielding three major fractions (Fr.A1–A3) (Fig. 3A). Among these, only Fr.A3 exhibited a significant reduction in HT-29 cell viability ($P < 0.01$), whereas Fr.A1 and Fr.A2 showed no detectable activity (Fig. 3B), indicating effective enrichment of the bioactive components in Fr.A3.

3.3.2 Anion-exchange chromatography reveals charge properties

Subsequent fractionation of Fr.A3 by anion-exchange chromatography demonstrated that the bioactivity was predominantly associated with fractions eluted at low ionic strength (~ 0.1 M NaCl) (Figs. 3C,D), suggesting weak binding affinity of the active components to the anion-exchange matrix. In contrast, no retention was observed during cation-exchange chromatography under acidic conditions (pH 5.0) (Fig. 3E), indicating that the active molecules do not possess a net positive charge. Collectively, these results suggest that the bioactive components carry a net negative charge under physiological conditions.

3.3.3 High-resolution purification of active fractions

Further refinement using linear gradient anion-exchange chromatography enabled high-resolution separation, with bioactivity confined to a limited subset of fractions (Fr.C11–C14) (Figs. 3F,G). These fractions exhibited the strongest inhibitory effects on cell viability ($P < 0.05$–0.01), indicating progressive enrichment of active components through sequential chromatographic procedures.

3.4 Parallel purification strategies reveal distinct active components

3.4.1 Liquid–liquid extraction indicates hydrophilic nature

Liquid–liquid extraction with ethyl acetate demonstrated that the anti-proliferative activity was retained exclusively in the aqueous phase ($P < 0.05$), whereas no detectable activity was observed in the organic phase (Fig. 4A). These results indicate that the active components are predominantly hydrophilic.

3.4.2 Activity distribution across molecular weight fractions

Subsequent ultrafiltration of the aqueous phase showed that both the > 10 kDa and < 10 kDa fractions retained anti-proliferative activity (Fig. 4B), suggesting that the aqueous extract contains multiple bioactive components with distinct molecular weight distributions.

3.4.3 Purification of > 10 kDa active component

Further separation of the > 10 kDa aqueous fraction by anion-exchange chromatography identified a major bioactive fraction, designated Fr.E15 (Figs. 4C–G). This result was consistent with the charge-related properties observed in the initial purification strategy, further supporting the association of anti-proliferative activity with negatively charged macromolecular components.

3.4.4 Isolation of a single active small-molecule fraction

Reverse-phase high-performance liquid chromatography (RP-HPLC) of the < 10 kDa fraction yielded a single predominant peak, Fr.F21, which exhibited strong anti-proliferative activity ($P < 0.001$) (Figs. 4H,I). These findings indicate that a highly purified low-molecular-weight bioactive component was successfully isolated through this parallel purification route.

3.5 LC–MS/MS analysis identifies proteins in active fractions

LC–MS/MS analysis was performed on three bioactive fractions (Fr.C11–14, Fr.E15, and Fr.F21) along with their corresponding inactive controls (Fr.C9, Fr.E12, and Fr.F25). Using a stringent false discovery rate (FDR) threshold of 1%, a total of 226 nonredundant proteins derived from *Bacteroides fragilis* were identified across all samples following high-confidence filtering, dataset integration, and deduplication.Quality assessment demonstrated a substantial improvement in precursor mass accuracy after calibration, with the majority of peptide-spectrum matches distributed within ± 5 ppm and centered around 0 ppm across all comparisons (Figs. 5A–C). Within the m/z range of 300–1400, mass errors remained stable without detectable systematic bias (Figs. 5D–F). Furthermore, more than 80% of the identified peptides exhibited no missed cleavages, indicating high digestion efficiency and overall data quality.Venn diagram analysis revealed that each bioactive fraction shared a subset of proteins with its corresponding inactive control, while also containing distinct, fraction-specific proteins (Figs. 5G–I). These results support the reliability of the proteomic dataset and provide a solid foundation for the subsequent identification of proteins associated with anti-proliferative activity.

3.6 Comparative proteomics reveals candidate functional proteins

3.6.1 Identification of enriched proteins

A total of 41 proteins were identified as significantly enriched in the bioactive fractions (Table 1). [Insert Table 1 approximately here] These proteins displayed a broad range of fold changes (up to 10^6) and molecular weights (31–127 kDa), with many exhibiting strong enrichment specificity relative to inactive controls.

3.6.2 Functional annotation and enrichment analysis

Gene Ontology (GO) analysis indicated that the enriched proteins were predominantly associated with membrane localization (> 90%), transport-related functions (43.9%), and processes related to iron acquisition and transmembrane transport (Figs. 6A–C).

Functional characterization of proteins enriched in bioactive fractions. (A–C) Gene Ontology (GO) enrichment analysis showing distributions across cellular component, molecular function, and biological process categories. (D) Predicted subcellular localization and secretion features of enriched proteins. (E) Functional association network of enriched proteins, where nodes represent proteins and edges indicate predicted functional relationships.

3.6.3 Protein family and structural features

Protein family classification revealed a marked enrichment of TonB-dependent receptors (24.4%), SusD family proteins (14.6%), and ATP-binding cassette (ABC) transporters (12.2%) (Table 2). [Insert Table 2 approximately here] These protein families are typically involved in nutrient uptake and membrane-associated transport systems.

3.6.4 Subcellular localization and secretion potential

A substantial proportion of the enriched proteins were predicted to localize to the outer membrane or extracellular interface, and several contained signal peptides indicative of secretion via classical pathways (Fig. 6D).

3.6.5 Functional interaction network

Network analysis identified five major functional modules, including iron transport, ABC transport systems, and protein secretion/processing pathways. Several hub proteins, such as BF9343_2013 and BF9343_1287, exhibited both high connectivity and strong enrichment, suggesting central roles within the functional network (Fig. 6E).

3.6.6 Candidate protein prioritization

Based on an integrated analysis incorporating enrichment level, functional annotation, predicted localization, and network centrality, five core candidate proteins were prioritized for further validation (Table 3).

Table 3
Candidate proteins prioritized based on integrated multi-criteria analysis

Rank	Protein name	FC	Subcellular localization	Network degree	Functional annotation	Integrated score
1	Transporter permease protein	1.05×10^6	Inner membrane	7	ABC transporter component	★★★★★
2	Signal peptidase I	1.56×10^5	Membrane-anchored	6	Protein processing enzyme	★★★★★
3	Ferrous iron transport protein B	1.10×10^5	Inner membrane	13	Iron transport protein	★★★★★
4	SusD family protein	2.19×10^4	Outer membrane	5	Carbohydrate-binding protein	★★★★★
5	Transport-related membrane protein	2.10×10^4	Inner membrane	3	Transport-associated protein	★★★★★

Candidate proteins prioritized based on integrated analysis. Selection criteria included enrichment, functional annotation, subcellular localization, and network connectivity. FC, fold change.

4. Discussion

An activity-guided fractionation strategy was applied in this study to systematically characterize the anti-proliferative components present in the culture supernatant of non-toxigenic *Bacteroides fragilis* (NTBF). By integrating ultrafiltration, size-exclusion chromatography, ion-exchange chromatography, and reverse-phase high-performance liquid chromatography with continuous bioactivity assessment, bioactive fractions were progressively enriched, enabling the correlation of chromatographic properties with functional activity.The findings indicate that the observed anti-colorectal cancer (CRC) effects are unlikely to be mediated by a single molecular entity. Instead, the bioactivity appears to arise from a multi-component system comprising both high- and low-molecular-weight fractions, which exhibit distinct physicochemical characteristics and may act in a coordinated or synergistic manner. Furthermore, the integration of fractionation with comparative proteomic analysis enabled the identification of a subset of proteins enriched in bioactive fractions, thereby providing mechanistic insights into the molecular basis of NTBF-associated tumor-suppressive effects.

Activity-guided fractionation remains a well-established and effective strategy for identifying bioactive components from complex biological mixtures[22, 23]. In contrast to conventional untargeted proteomics, this approach offers the distinct advantage of directly associating biological activity with fractionation behavior, thereby facilitating the exclusion of highly abundant but functionally irrelevant molecules[24]. This advantage is particularly relevant for microbial secretomes, which comprise complex mixtures of proteins, metabolites, and other extracellular components, in which low-abundance bioactive factors may otherwise remain undetected[25].At the same time, several methodological limitations should be acknowledged, Multi-step chromatographic purification is inherently labor-intensive and may result in partial activity loss due to repeated handling, dilution, or degradation of labile molecules during processing[26]. More importantly, activity-guided fractionation has traditionally been optimized for the isolation of a single dominant bioactive compound, In the present study, however, the anti-CRC activity associated with NTBF appeared to involve multiple components, suggesting that functionally relevant effects may depend not only on individual molecules but also on their combinatorial or cooperative interactions, Under such circumstances, conventional purification strategies may disrupt native associations among active factors and

thereby underestimate their biological effects[27].To address this challenge, two parallel purification routes were implemented, each combined with stepwise bioactivity validation, in order to improve the robustness of fraction tracking and reduce the likelihood of stochastic activity loss. Nevertheless, further methodological refinement will be required to better preserve native bioactive interactions. Future studies may benefit from the use of milder separation conditions, orthogonal co-fractionation strategies, or interaction-preserving approaches that allow multi-component systems to be characterized more faithfully in their functional state.

One of the most notable findings of this study is that anti-proliferative activity was retained in both the > 10 kDa and < 10 kDa fractions following ethyl acetate extraction and ultrafiltration. This result suggests that the bioactive components are unlikely to exist as a single, structurally uniform entity and instead may reflect a more complex molecular organization or processing pattern.Several non-mutually exclusive mechanisms may account for this observation. One possible explanation is a precursor-to-active-fragment model, in which larger proteins serve as precursors for smaller bioactive peptides generated through proteolytic processing. Such mechanisms have been widely described in bacteria, where functionally active peptides are produced by post-translational cleavage of larger protein substrates[28]. In this context, the detection of putative proteases, such as BF9343_3187, in the bioactive fractions provides indirect support for this possibility. A second explanation is that the active factors may exist as higher-order protein complexes under native conditions. During extraction and chromatographic separation, changes in physicochemical parameters, including pH, ionic strength, and molecular dilution, may have promoted partial or complete dissociation of these complexes, thereby releasing smaller subunits that retained biological activity. This interpretation is consistent with the possibility that fractionation altered the native structural state of the active system without fully abolishing its functional properties[29].A third possibility is that the observed activity reflects a multi-component synergistic model. Under this scenario, molecules of different molecular weights may act on distinct cellular targets or signaling pathways, and their combined actions may generate a stronger anti-proliferative effect than any individual component alone. Such a model would also be consistent with the broader view that microbial secretomes function as integrated bioactive systems rather than as collections of isolated single-effect molecules[29, 30]. Taken together, these interpretations emphasize the molecular complexity of NTBF-derived bioactivity and suggest that the anti-CRC effects observed in this study may arise from multiple interacting components rather than from a single effector. Further investigation will therefore be required to distinguish among these possibilities, particularly through proteolytic mapping, activity reconstitution experiments, and structural characterization of native and fractionated bioactive components.

Ion-exchange chromatography demonstrated that the bioactive components were retained on anion-exchange matrices but not on cation-exchange columns under near-physiological pH conditions, indicating that these molecules possess a net negative charge[31]. This finding is consistent with the predicted isoelectric point distribution of the enriched proteins and is in agreement with previous reports showing preferential enrichment of acidic proteins in *Bacteroides*-derived outer membrane vesicles (OMVs) and secretion systems.In addition, ethyl acetate extraction revealed that the anti-proliferative activity was exclusively confined to the aqueous phase, indicating a predominantly hydrophilic nature. This physicochemical property further supports the interpretation that the active components are proteinaceous or peptide-based, rather than hydrophobic small-molecule metabolites.Taken together, these results support a model in which the anti-colorectal cancer activity associated with NTBF is primarily mediated by secreted or surface-associated proteins, potentially linked to OMVs or extracellular transport mechanisms, thereby highlighting a functional role for protein-mediated host–microbe interactions in tumor suppression[32, 33].

Comparative proteomic analysis identified 41 proteins significantly enriched in the bioactive fractions, which were not randomly distributed but instead organized into distinct functional modules. Among these, the enrichment of TonB-dependent receptors and iron acquisition–related proteins is particularly notable. Colorectal cancer cells, like many tumor types, exhibit a strong dependence on iron to sustain rapid proliferation, a phenomenon often described as “iron addiction[34],” characterized by enhanced iron uptake and reprogramming of iron metabolism[35]. In parallel, gut commensals have evolved highly efficient iron acquisition systems to compete within iron-limited host environments[36]. *Bacteroides* species, in particular, employ TonB-dependent transporters and siderophore-associated pathways to capture iron sources such as heme and ferrichrome[37]. Based on these observations, a nutrient competition model is proposed, whereby NTBF-derived factors sequester extracellular iron, thereby creating a localized iron-restricted microenvironment that may limit CRC cell proliferation.Beyond metabolic competition, several enriched proteins—including outer membrane proteins and SusD family polysaccharide-binding proteins—suggest the involvement of direct host–microbe interactions, These proteins are typically localized to the bacterial surface or associated with outer membrane vesicles (OMVs) and may interact with host epithelial or immune cells, thereby modulating signaling pathways and cellular responses relevant to tumor progression[38, 39]. Furthermore, the enrichment of ATP-binding cassette (ABC) transporters and components of the Sec secretion system indicates the presence of a coordinated protein production, processing, and secretion network. This observation supports the interpretation that the

observed bioactivity is mediated, at least in part, by actively secreted bacterial effectors rather than passive byproducts[40–42].Taken together, these findings support a dual mechanistic framework in which NTBF-derived anti-CRC activity may arise from the combined effects of nutrient competition and direct host–microbe interactions. This integrated model provides a more comprehensive basis for understanding how commensal bacteria modulate tumor-associated processes at both metabolic and molecular levels.

This study provides several important advances. First, an integrated analytical framework was established that combines activity-guided fractionation, quantitative proteomics, and network-based functional analysis, enabling systematic identification of bioactive components within a complex microbial secretome. Second, the findings support a multi-component and multi-mechanistic model of anti-colorectal cancer (CRC) activity, moving beyond the traditional single-molecule paradigm and more accurately reflecting the complexity of host–microbe interactions. Third, a mechanistic hypothesis is proposed linking microbial iron competition and membrane-associated protein interactions to tumor suppression, thereby expanding current conceptual models of microbiota-mediated cancer regulation.Despite these strengths, several limitations should be considered. The current conclusions are largely based on correlative proteomic data, and direct functional validation of key candidate proteins (e.g., BF9343_2013 and BF9343_3187) remains necessary through approaches such as gene knockout, recombinant expression, or activity reconstitution. In addition, the downstream molecular mechanisms in CRC cells—particularly those involving cell cycle regulation, apoptosis, and specific signaling pathways—have not yet been fully elucidated. Furthermore, all experiments were conducted in vitro, and the in vivo efficacy, bioavailability, and safety of the identified components require evaluation in appropriate animal models. Finally, the proteomics-centered approach may not fully capture the potential contributions of non-protein factors, such as polysaccharides or lipid-derived molecules, which could also participate in the observed bioactivity.Future investigations should therefore focus on comprehensive functional validation of prioritized hub proteins, integration of multi-omics approaches (e.g., transcriptomics and phosphoproteomics), and validation in in vivo CRC models. In parallel, detailed structural and biochemical characterization of key bioactive molecules will be essential. Collectively, these efforts will be critical for advancing the mechanistic understanding of NTBF-derived anti-tumor activity and facilitating its translation into potential therapeutic applications.

5. Conclusions

In this study, an integrated activity-guided fractionation and proteomic approach was applied to systematically identify proteins associated with the anti-colorectal cancer activity of a human-derived non-enterotoxigenic *Bacteroides fragilis* strain.A total of 41 candidate proteins were identified, with enrichment primarily observed in pathways related to iron acquisition, ATP-binding cassette (ABC) transport, and protein secretion. A substantial proportion of these proteins were predicted to localize to the outer membrane or to possess secretion signals, indicating their potential involvement in extracellular or host-interactive functions.Collectively, these results suggest that the observed anti-tumor activity is not attributable to a single effector molecule but is more likely mediated by a coordinated multi-component protein system. This study provides a systematic framework for identifying microbiota-derived anti-cancer factors and offers new mechanistic insights into the role of commensal bacteria in modulating colorectal cancer.

Declarations

Author contributions

YP and JL conceptualized and designed the study. YP performed the experiments and collected the data. YP, LH, and MC analyzed the proteomic data. HY, YG, and NW performed the bioinformatics analysis. MW and ZY contributed to the interpretation of the data. YP wrote the original manuscript draft. JL, LH, and MC reviewed and edited the manuscript. JL supervised the study and acquired the funding. All authors read and approved the final manuscript.

Funding

This work was supported by Natural Science Research Project of Guizhou Education Department in 2024 (Guizhou Education Technology [2024] No. 335), the financial support from the Zunyi city Science and Technology Program project (Zunyi City, Kehe HZ character (2024) No. 303), Zunyi Science and Technology Innovation Team for Nutrition and Health (Project No.: Zun KCTD [2025] 89), Scientific Research Program of Guizhou Provincial Department of Education (QJJ [2023] 019), and the National Science and Technology Innovation 2030, Noncommunicable Chronic Diseases-National Science and Technology Major Project (GrantN0.2024ZD0524300.2024ZD0524304), Governor's Special Fund for Outstanding Scientific and Technological Education Talents in Guizhou Province (No. [2011]57).

Data availability

All data generated or analyzed during this study are included in this published article and its supplementary information files.

Ethical approval and consent to participate

Not applicable. This study did not involve human participants, human data, or animal experiments. The HT-29 colorectal cancer cell line used in this study was obtained from a commercial cell bank (Cell Bank of the Chinese Academy of Sciences).

Competing interests

The authors declare that they have no competing interests.

Consent for publication statement

Not applicable.

References

1. BRAY F, LAVERSANNE M. Global cancer statistics 2022: GLOBOCAN estimates of incidence and mortality worldwide for 36 cancers in 185 countries [J]. Cancer J Clin. 2024;74(3):229–63.
2. LI J, MA X. Genetic and biological hallmarks of colorectal cancer [J]. Genes Dev. 2021;35(11–12):787–820.
3. SIEGEL R L SUNGH, LAVERSANNE M, et al. Colorectal cancer incidence trends in younger versus older adults: an analysis of population-based cancer registry data [J]. Lancet Oncol. 2025;26(1):51–63.
4. Global. regional, and national burden of colorectal cancer and its risk factors, 1990–2019: a systematic analysis for the Global Burden of Disease Study 2019 [J]. Volume 7. The lancet Gastroenterology & hepatology; 2022. pp. 627–47. 7.
5. MORGAN E, ARNOLD M. Global burden of colorectal cancer in 2020 and 2040: incidence and mortality estimates from GLOBOCAN [J]. Gut. 2023;72(2):338–44.
6. CERVANTES A, ADAM R, ROSELLó S, et al. Metastatic colorectal cancer: ESMO Clinical Practice Guideline for diagnosis, treatment and follow-up [J]. Annals oncology: official J Eur Soc Med Oncol. 2023;34(1):10–32.
7. BARATHAN M, ZULPA A K, NG SL et al. Innovative Strategies to Combat 5-Fluorouracil Resistance in Colorectal Cancer: The Role of Phytochemicals and Extracellular Vesicles [J]. Int J Mol Sci, 2024, 25(13).
8. DIAZ L A JR, SHIU K K, KIM T W, et al. Pembrolizumab versus chemotherapy for microsatellite instability-high or mismatch repair-deficient metastatic colorectal cancer (KEYNOTE-177): final analysis of a randomised, open-label, phase 3 study [J]. Lancet Oncol. 2022;23(5):659–70.
9. LI J, ZHU J X, ZHANG Y X, et al. Effectiveness of immune checkpoint inhibitors in combination with tyrosine kinase inhibitors in patients with advanced or metastatic colorectal carcinoma with either mismatch repair proficient or metastatic microsatellite stable disease: A systematic review and meta–analysis [J]. Oncol Lett. 2024;27(4):153.
10. SMET A, KUPCINSKAS J, LINK A, et al. The Role of Microbiota in Gastrointestinal Cancer and Cancer Treatment: Chance or Curse? [J]. Cell Mol Gastroenterol Hepatol. 2022;13(3):857–74.
11. GUO C, WANG C. Microbiota-host metabolism reprogramming in colorectal cancer: from pathogenesis to precision therapies [J]. Front Oncol. 2025;15:1713614.
12. MEHTA A, VASUDEVAN S, SACHDEVA N et al. Gut metabolite alterations in colorectal cancer: Fecal analysis of short-chain fatty acids and secondary bile acids [J]. 2025, 17(1).
13. VIDAL-VEUTHEY B, GONZáLEZ D, CáRDENAS JP. Role of microbial secreted proteins in gut microbiota-host interactions [J]. 2022, Volume 12–2022.
14. CHUNG Y, RYU Y, AN B C, et al. A synthetic probiotic engineered for colorectal cancer therapy modulates gut microbiota [J]. Microbiome. 2021;9(1):122.
15. YANG Y, CAO X. KATO N, et al. Gut Bacteroides fragilis in health and diseases: An updated review [J]. Journal of Future Foods; 2025.
16. JASEMI S, MOLICOTTI P, FAIS M et al. Biological Mechanisms of Enterotoxigenic Bacteroides fragilis Toxin: Linking Inflammation, Colorectal Cancer, and Clinical Implications [J]. Toxins, 2025, 17(6).

17. SCOTT N, WHITTLE E, JERALDO P, et al. A systemic review of the role of enterotoxic Bacteroides fragilis in colorectal cancer [J]. Volume 29. Neoplasia (New York, NY); 2022. p. 100797.
18. XIA S, MA L, LI H, et al. Prevalence of enterotoxigenic Bacteroides fragilis in patients with colorectal cancer: a systematic review and meta-analysis [J]. Front Cell Infect Microbiol. 2025;15:1525609.
19. ARNOLDS K L YAMADAE, NEFF C P, et al. Disruption of Genes Encoding Putative Zwitterionic Capsular Polysaccharides of Diverse Intestinal Bacteroides Reduces the Induction of Host Anti-Inflammatory Factors [J]. Microb Ecol. 2023;85(4):1620–9.
20. ZHONG Y, CHANG X, ZHAO Z, et al. Bacteroides fragilis capsular polysaccharide A ameliorates ulcerative colitis in rat by recovering intestinal barrier integrity and restoring gut microbiota [J]. Front Pharmacol. 2024;15:1402465.
21. YANG H, GAN Y, JIANG S, et al. Genomic alterations in Bacteroides fragilis favor adaptation in colorectal cancer microenvironment [J]. BMC Genomics. 2025;26(1):269.
22. PUTRA M Y, YULIANA N D, FIRDAUS R et al. Bridging Bioassay-Guided Isolation and Metabolomics: Toward Hybrid Strategies in Natural Product Drug Discovery [J]. ChemRxiv, 2026(0128).
23. STRöMSTEDT AA, FELTH J. Bioassays in natural product research - strategies and methods in the search for anti-inflammatory and antimicrobial activity [J]. Phytochem Anal. 2014;25(1):13–28.
24. MIURA N. Current progress and critical challenges to overcome in the bioinformatics of mass spectrometry-based metaproteomics [J]. Comput Struct Biotechnol J. 2023;21:1140–50.
25. RIGHETTI BOSCHETTIE. P G. Low-Abundance Protein Enrichment for Medical Applications: The Involvement of Combinatorial Peptide Library Technique [J]. Int J Mol Sci, 2023, 24(12).
26. HAN C, WANG S, LI Z, et al. Bioactivity-guided cut countercurrent chromatography for isolation of lysine-specific demethylase 1 inhibitors from Scutellaria baicalensis Georgi [J]. Anal Chim Acta. 2018;1016:59–68.
27. KELLOGG JJ, PAINE M F, MCCUNE JS, et al. Selection and characterization of botanical natural products for research studies: a NaPDI center recommended approach [J]. Nat Prod Rep. 2019;36(8):1196–221.
28. LI H, DING W. Discovery and engineering of ribosomally synthesized and post-translationally modified peptide (RiPP) natural products [J]. RSC Chem biology. 2024;5(2):90–108.
29. SHAHNAWAZ M. Microcin amyloid fibrils A are reservoir of toxic oligomeric species [J]. J Biol Chem. 2012;287(15):11665–76.
30. CHOU TC. Theoretical basis, experimental design, and computerized simulation of synergism and antagonism in drug combination studies [J]. Pharmacol Rev. 2006;58(3):621–81.
31. GRODZKI A C BERENSTEINE. Antibody purification: ion-exchange chromatography [J]. (Clifton NJ). 2010;588:27–32. Methods in molecular biology.
32. ELHENAWY W, DEBELYY MYKHAYLO O, FELDMAN MARIO F. Preferential Packing of Acidic Glycosidases and Proteases into Bacteroides Outer Membrane Vesicles [J]. mBio. 2014;5(2). 10.1128/mbio.00909 - 14.
33. BYUN H, PARK J, KIM S C, et al. A lower isoelectric point increases signal sequence-mediated secretion of recombinant proteins through a bacterial ABC transporter [J]. J Biol Chem. 2017;292(48):19782–91.
34. RODRIGUEZ R, SCHREIBER S L CONRADM. Persister cancer cells: Iron addiction and vulnerability to ferroptosis [J]. Mol Cell. 2022;82(4):728–40.
35. ESTêVãO D, DA CRUZ-RIBEIRO M, CARDOSO A P, et al. Iron metabolism in colorectal cancer: a balancing act [J]. Cell Oncol (Dordrecht Netherlands). 2023;46(6):1545–58.
36. XIAO L, TANG R, WANG J, et al. Gut microbiota bridges the iron homeostasis and host health [J]. Sci China Life Sci. 2023;66(9):1952–75.
37. PARKER A C, SEALS N L, BACCANALE C L, et al. Analysis of Six tonB Gene Homologs in Bacteroides fragilis Revealed That tonB3 is Essential for Survival in Experimental Intestinal Colonization and Intra-Abdominal Infection [J]. Infect Immun. 2022;90(1):e0046921.
38. BROWN H A, KOROPATKIN NM. Host glycan utilization within the Bacteroidetes Sus-like paradigm [J]. Glycobiology. 2021;31(6):697–706.
39. GILMORE W J, JOHNSTON E L, BITTO NJ, et al. Bacteroides fragilis outer membrane vesicles preferentially activate innate immune receptors compared to their parent bacteria [J]. Front Immunol. 2022;13:970725.
40. AKHTAR A A, TURNER DP. The role of bacterial ATP-binding cassette (ABC) transporters in pathogenesis and virulence: Therapeutic and vaccine potential [J]. Microb Pathog. 2022;171:105734.

41. HOW SS, LAM NATHANS. ATP-binding cassette (ABC) transporters: structures and roles in bacterial pathogenesis [J]. J Zhejiang Univ Sci B. 2024;26(1):58–75.
42. TSIRIGOTAKI A, DE GEYTER J, ŠOŠTARIC N, et al. Protein export through the bacterial Sec pathway [J]. Nat Rev Microbiol. 2017;15(1):21–36.

Tables

Table 1
Proteins significantly enriched in active fractions

No	Accession	Gene ID	Protein name	FC	MW (kDa)	Coverage (%)	Localization	Functional category
1	Q5LDL5	BF9343_2013	Transporter permease protein	1049815.0	91	3.1	IM	ABC transporter
2	Q5LB38	BF9343_2903	Signal peptidase I	155762.8	34	1.7	MEM	Secretion
3	Q5LFM5	BF9343_1287	Ferrous iron transport protein B	110201.1	93	2.9	IM	Iron uptake
4	Q5LH33	BF9343_0772	Hexuronate transporter	66678.0	53	1.7	IM	MFS transporter
5	Q5L8Z0	BF9343_3661	Transport-related membrane protein	29076.4	48	3.6	IM	ABC transporter
6	Q5LA73	BF9343_3220	Exported protein (SusD)	21912.0	71	1.5	OM	SusD family
7	Q5LE18	cydA BF9343_1854	Cytochrome d oxidase subunit I	14938.7	58	1.7	IM	Energy metabolism
8	Q5LDC0	BF9343_2109	Lipoprotein (SusD)	12975.6	50	3.2	OM-LP	SusD family
9	A0A380YP97	BF9343_2893	ABC transport system, membrane protein	12971.8	65	1.9	IM	ABC transporter
10	Q5L839	BF9343_3977	Fimbrillin-A associated protein	11055.5	31	2.1	OM	Cell wall
11	Q5L7G2	BF9343_4209	TonB-dependent receptor	8086.6	119	0.8	OM	Iron uptake
12	Q5LAK0	BF9343_3092	2,6-β-D-fructofuranosidase	7347.3	88	1.5	OM	Glycosidase
13	Q5L8Z3	BF9343_3658	Outer membrane protein (OMF family)	5870.3	53	1.0	OM	Efflux pump
14	A0A380YZ17	mobC BF9343_1444	Mobilisation protein C	5179.2	61	1.3	IM	Conjugation
15	Q5LDM5	BF9343_2002	Transmembrane cation-transporting ATPase	5021.4	80	1.0	IM	Copper transport
16	Q5LDW5	BF9343_1909	Outer membrane protein	5018.1	127	1.2	OM	Iron uptake
17	A0A380YWY0	BF9343_0478	Outer membrane protein	2660.8	118	0.4	OM	Iron uptake
18	Q5LIC9	BF9343_0318	TonB-dependent receptor exported protein	3.6	95	1.6	OM	Iron uptake
19	Q5LDV7	BF9343_1917	Polysialic acid capsule transport protein	2612.9	80	1.2	OM	Capsule transport
20	Q5L7F5	BF9343_4216	Transmembrane ion channel	2451.1	68	1.2	IM	Ion channel
21	Q5LHU6	kdpB BF9343_0505	Potassium-transporting ATPase subunit B	1770.5	73	1.5	IM	Ion transport
22	Q5LEJ4	BF9343_1676	Transmembrane TraG/TraD family protein	1086.3	76	2.8	IM	Conjugation

No	Accession	Gene ID	Protein name	FC	MW (kDa)	Coverage (%)	Localization	Functional category
23	Q5LDA2	BF9343_2127	ABC transport system, membrane protein	1070.7	87	1.3	IM	ABC transporter
24	Q5LAX2	ffh BF9343_2970	Signal recognition particle protein	1015.2	49	1.4	CP	Protein targeting
25	A0A380Z384	BF9343_1437	Outer membrane protein	16.0	126	1.0	OM	Iron uptake
26	Q5LIT0	BF9343_0167	histidine kinase	6.8	52	2.4	IM	Signaling
27	A0A380YU57	BF9343_4043	histidine kinase	6.2	62	4.9	IM	Signaling
28	Q5LHT8	frrH BF9343_0513	Outer membrane protein (SusD family)	5.6	56	2.0	OM	SusD family
29	Q5LA44	BF9343_3249	K+ transport related protein	5.3	84	1.2	IM	Ion transport
30	Q5LHL9	BF9343_0582	ATP-binding transporter component	4.4	83	2.2	IM	ABC transporter
31	Q5L928	BF9343_3623	Exported protein (TonB-dependent)	3.4	123	2.1	OM	Iron uptake
32	Q5L857	BF9343_3955	TonB-linked outer membrane protein	3.1	110	0.9	OM	Iron uptake
33	Q5L929	BF9343_3622	Uncharacterized protein (SusD family)	2.9	61	1.7	OM	SusD family
34	Q5LHC4	BF9343_0677	TonB-dependent receptor	2.9	104	0.4	OM	Iron uptake
35	Q5LAA5	sppA BF9343_3187	Protease IV	2.7	65	1.0	MEM	Secretion
36	A0A380Z304	BF9343_1344	Outer membrane protein	2.6	126	0.8	OM	Iron uptake
37	Q5LD69	BF9343_2160	Iron transport membrane protein	2.6	36	5.8	IM	Iron uptake
38	Q5LAM6	BF9343_3066	Exported protein (OMF family)	2.1	48	0.9	OM	Efflux pump
39	Q5LGV4	BF9343_0851	Uncharacterized protein (SusD family)	2.0	77	1.3	OM	SusD family
40	Q5LGV2	BF9343_0854	Uncharacterized protein (SusD family)	2.0	78	1.3	OM	SusD family
41	Q5LIJ2	ftsI pbpB BF9343_0255	Cell division transpeptidase	2.0	77	3.9	IM	Cell wall synthesis

Proteins are significantly enriched in bioactive fractions. Proteins are ranked according to fold change (FC). MW, molecular weight; Coverage, sequence coverage.

Table 2
Protein family classification of enriched proteins

Protein family	Number	Percentage (%)	Representative proteins	Functional category
TonB-dependent receptors	10	24.4	BF9343_3623, BF9343_1909, BF9343_1344, BF9343_1437, BF9343_0478, BF9343_0318, BF9343_0677, BF9343_4209, BF9343_3955, BF9343_3092	Transport (iron uptake, nutrient import)
SusD family proteins	6	14.6	BF9343_3220, BF9343_0851, BF9343_0854, BF9343_3622, BF9343_2109, BF9343_3658	Carbohydrate binding and uptake
ABC transporter-related proteins	5	12.2	BF9343_2013, BF9343_3661, BF9343_2127, BF9343_0582, BF9343_2893	ATP-dependent transport
Ion transport/channel proteins	4	9.8	BF9343_4216, BF9343_3249, BF9343_2002, BF9343_0505	Ion transport
Enzymes (processing-related)	3	7.3	BF9343_2903, BF9343_3187, BF9343_2970	Protein processing
Respiratory chain components	2	4.9	BF9343_1854, BF9343_0772	Energy metabolism
Signal transduction-related proteins	2	4.9	BF9343_4043, BF9343_0167	Signal transduction
Cell division-related proteins	2	4.9	BF9343_0255, BF9343_3977	Cell division
Others / unclassified	7	17.1	BF9343_3066, BF9343_0857, BF9343_1444, etc.	Uncharacterized

Protein family classification of enriched proteins. Families were assigned based on database annotations, with values representing the number and proportion of proteins in each category.

Figures

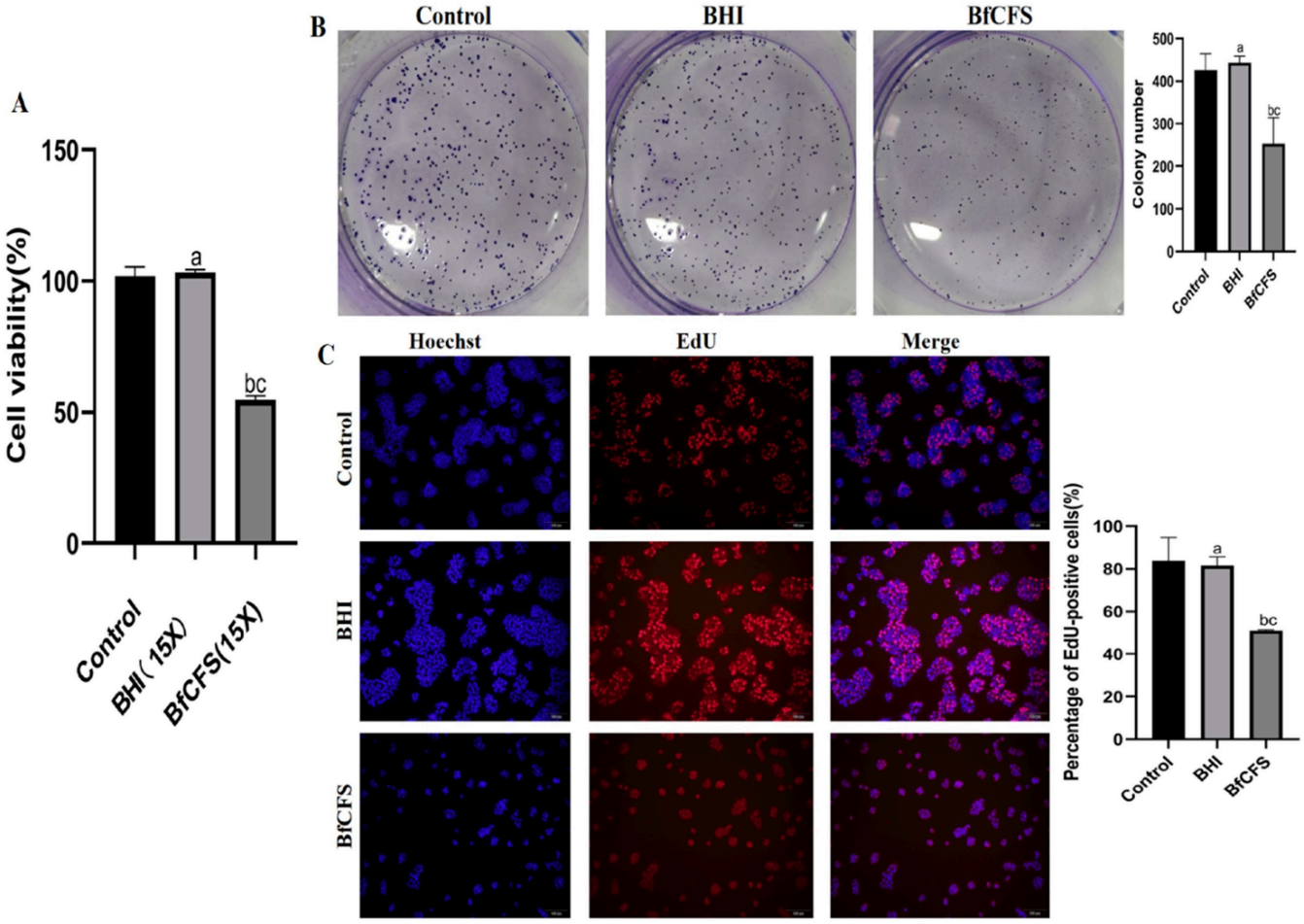


Figure 1

Cell-free supernatant derived from *Bacteroides fragilis* ZY0804 (BfCFS) inhibits the proliferation of HT-29 colorectal cancer cells. (A) CCK-8 assay showing the effect of BfCFS on cell viability. (B) Colony formation assay illustrating the impact of BfCFS on clonogenic growth. (C) EdU incorporation assay showing the effect of BfCFS on DNA synthesis and proliferative activity, including representative fluorescence images and quantitative analysis. Data are presented as mean ± SD from three independent experiments (n = 3). a, $P > 0.05$ vs. control; b, $P < 0.001$ vs. control in panels A and C, and $P < 0.01$ vs. control in panel B; c, $P < 0.001$ vs. BHI in panels A and C, and $P < 0.01$ vs. BHI in panel B.

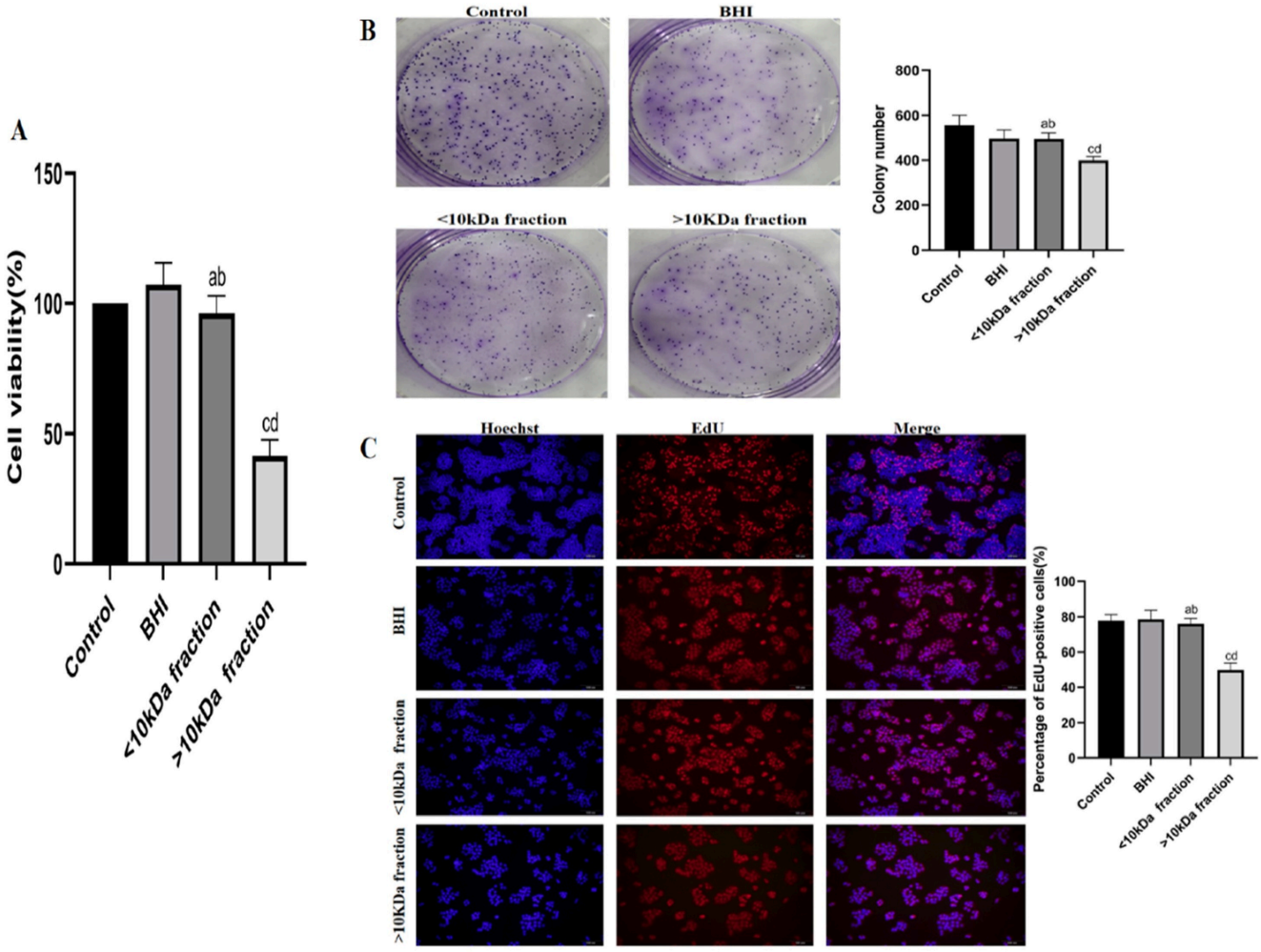


Figure 2

Anti-proliferative activity of BfCFS is primarily associated with fractions >10 kDa. (A) CCK-8 assay evaluating the effects of <10 kDa and >10 kDa fractions on HT-29 cell viability. (B) Colony formation assay assessing the impact of different molecular weight fractions on clonogenic growth. (C) EdU incorporation assay showing the effects of these fractions on DNA synthesis and proliferative activity, including representative fluorescence images and quantitative analysis. Data are presented as mean ± SD from three independent experiments (n = 3). a, $P > 0.05$ vs. control; b, $P > 0.05$ vs. BHI; c, $P < 0.001$ vs. control; d, $P < 0.001$ vs. BHI (in panel B, d indicates $P < 0.01$ vs. BHI).

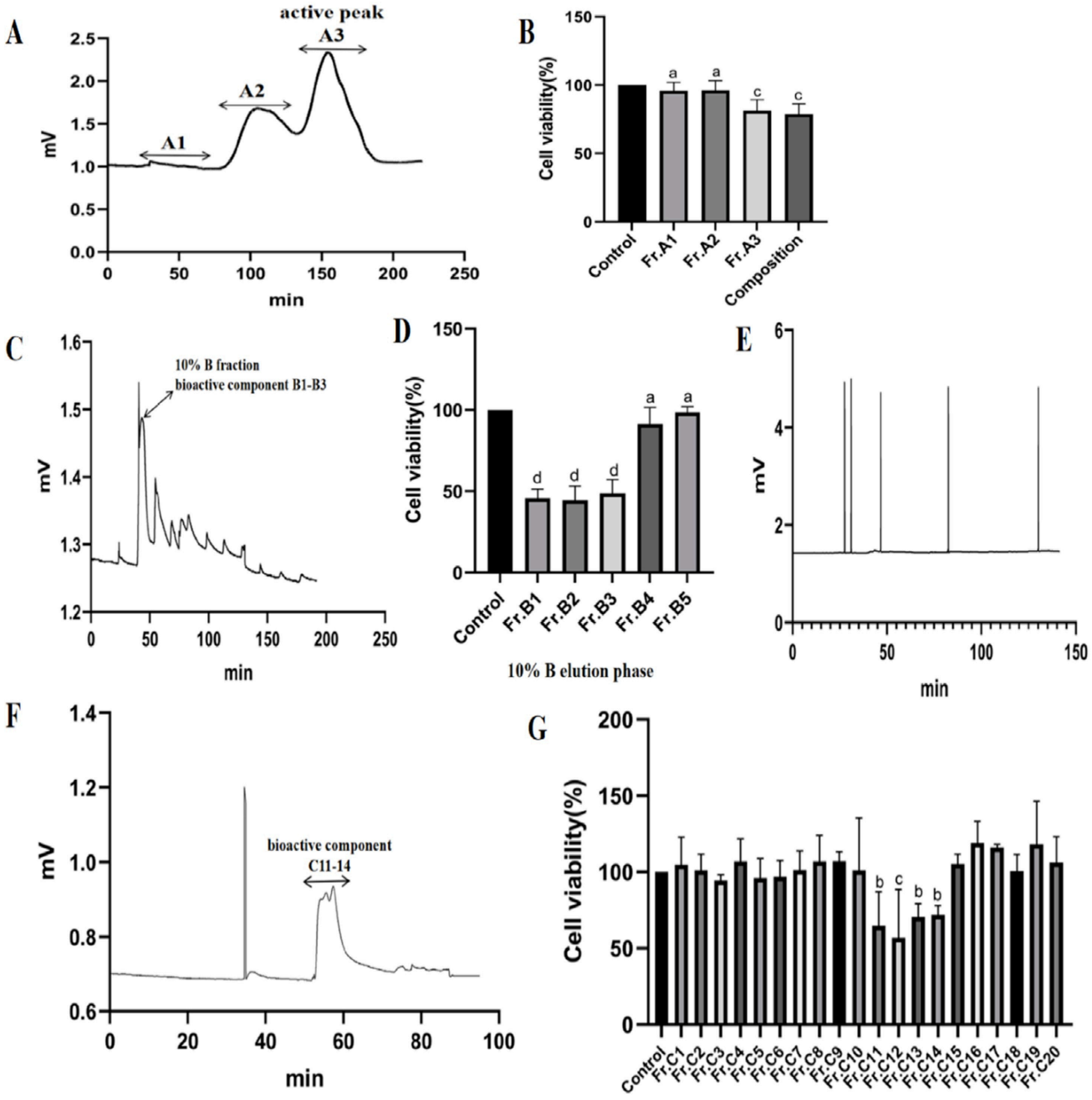


Figure 3

Sequential chromatographic fractionation enriches bioactive components from BfCFS. (A) Size-exclusion chromatography (Sephacryl S-200) profile of the >10 kDa fraction, showing separation into three major fractions (Fr.A1–A3). (B) CCK-8 assay evaluating the effects of SEC fractions on HT-29 cell viability. (C) Anion-exchange chromatography profile (HiTrap Q HP) of Fr.A3 under stepwise gradient elution. (D) CCK-8 assay showing the distribution of anti-proliferative activity across collected fractions. (E) Cation-exchange chromatography profile (HiTrap SP HP) illustrating the binding behavior of Fr.A3 under acidic conditions. (F) Linear gradient anion-exchange chromatography profile for high-resolution separation. (G) CCK-8 assay evaluating the activity of fractions obtained from gradient elution. Data are presented as mean ± SD from three independent experiments (n = 3). a, $P > 0.05$ vs. control; b, $P < 0.05$ vs. control; c, $P < 0.01$ vs. control; d, $P < 0.001$ vs. control.

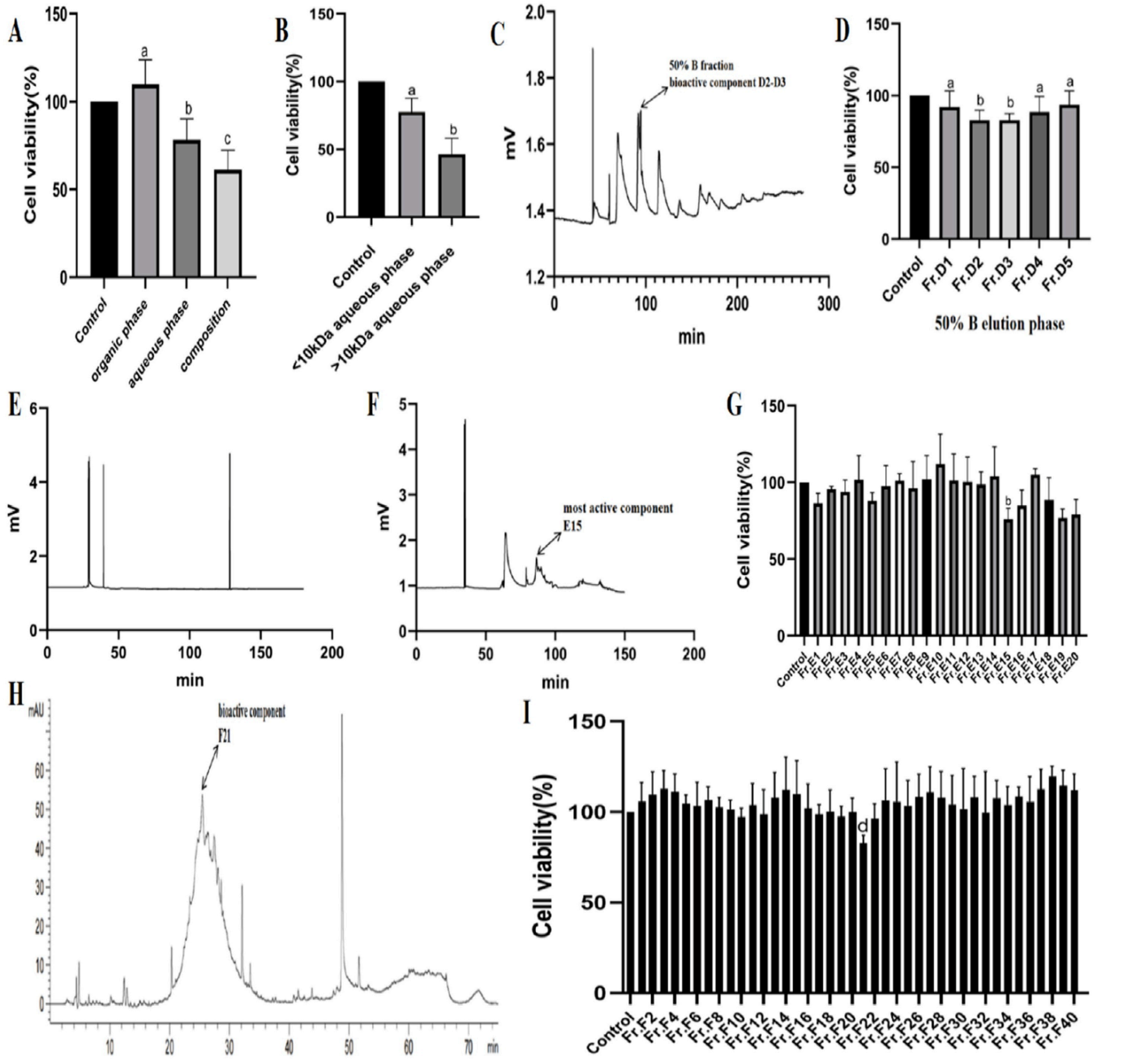


Figure 4

Parallel fractionation strategies identify distinct bioactive components in the aqueous fraction of BfCFS.(A) CCK-8 assay showing the effects of the aqueous and organic phases after ethyl acetate extraction on HT-29 cell viability. (B) CCK-8 assay evaluating the effects of the <10 kDa and >10 kDa fractions derived from the aqueous phase on HT-29 cell viability. (C) Anion-exchange chromatography profile (HiTrap Q HP) of the >10 kDa aqueous fraction under stepwise gradient elution. (D) CCK-8 assay showing the distribution of anti-proliferative activity among fractions collected from anion-exchange chromatography. (E) Cation-exchange chromatography profile (HiTrap SP HP) illustrating the binding behavior of the >10 kDa fraction under acidic conditions. (F) Linear gradient anion-exchange chromatography profile for high-resolution separation of active components. (G) CCK-8 assay showing the activity of fractions obtained

from gradient elution. (H) RP-HPLC chromatogram showing the separation profile of the <10 kDa fraction. (I) CCK-8 assay evaluating the activity of fractions collected after RP-HPLC separation. Data are presented as mean ± SD from three independent experiments (n = 3). a, P > 0.05 vs. control; b, P < 0.05 vs. control; c, P < 0.01 vs. control; d, P < 0.001 vs. control.

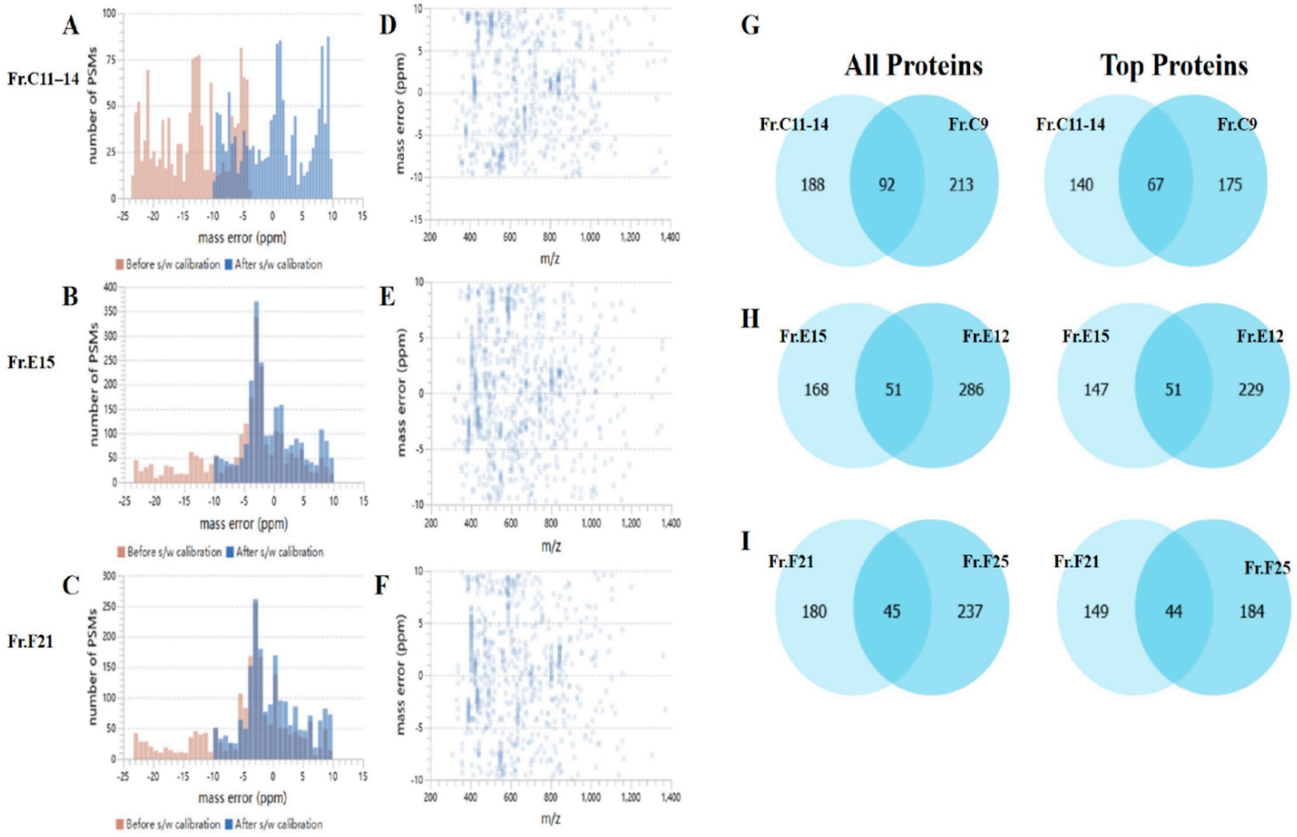


Figure 5

Quality assessment and protein identification overview of LC–MS/MS datasets from active and inactive fractions.(A–C) Distributions of precursor mass errors for filtered peptide-spectrum matches before and after calibration in the Fr.C11–14/Fr.C9, Fr.E15/Fr.E12, and Fr.F21/Fr.F25 comparisons, respectively. (D–F) Scatter plots illustrating the relationship between precursor m/z and mass error for the three active–inactive fraction pairs. (G–I) Venn diagrams showing the overlap and fraction-specific distribution of identified proteins between each bioactive fraction and its corresponding inactive control.

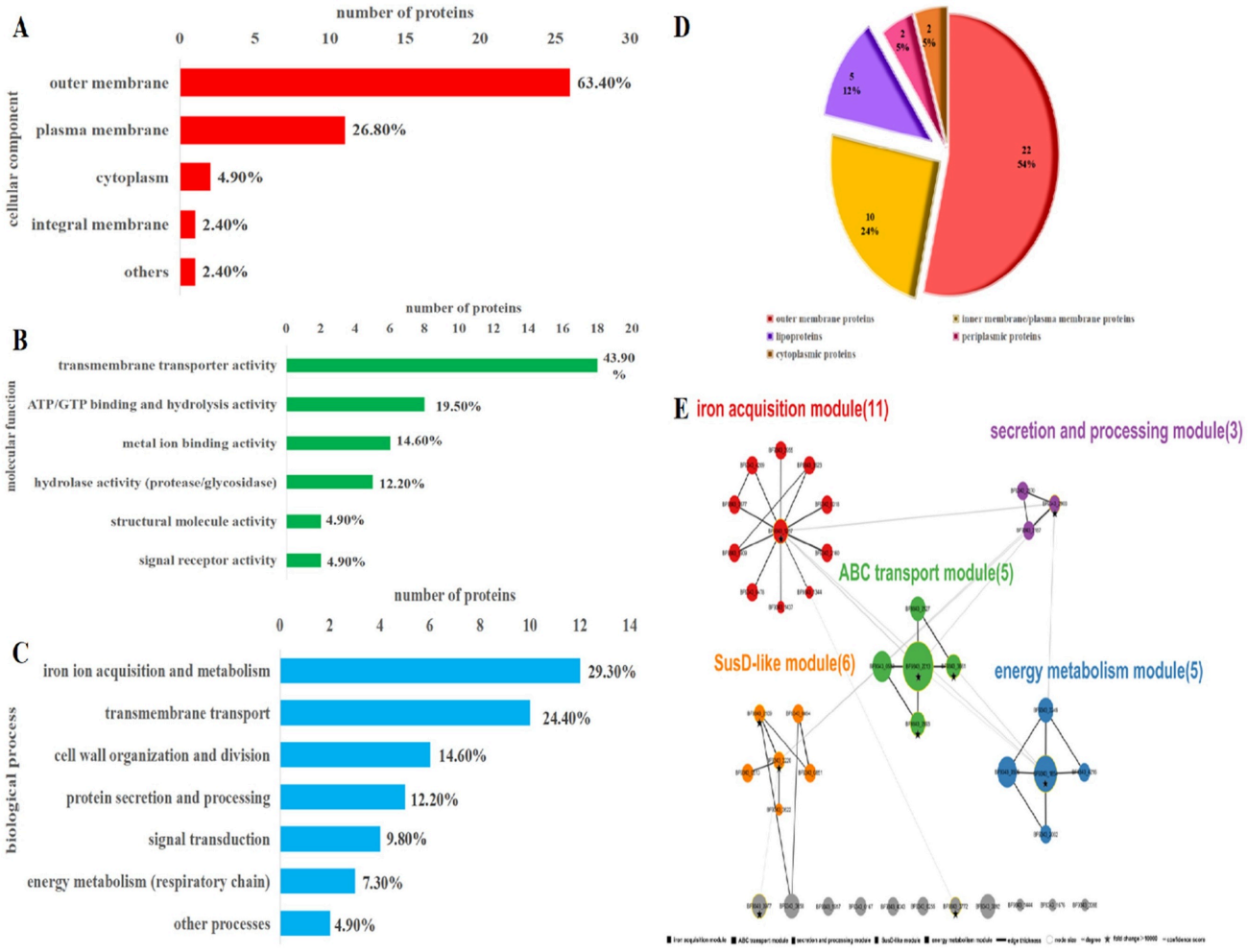


Figure 6

Functional characterization of proteins enriched in active fractions.

Functional characterization of proteins enriched in bioactive fractions. (A–C) Gene Ontology (GO) enrichment analysis showing distributions across cellular component, molecular function, and biological process categories. (D) Predicted subcellular localization and secretion features of enriched proteins. (E) Functional association network of enriched proteins, where nodes represent proteins and edges indicate predicted functional relationships.

Supplementary Files

This is a list of supplementary files associated with this preprint. Click to download.

- SupplementaryTableS1.zip